Internal Phase Separation Drives Dewetting in Polymer Blend and Nanocomposite Films

Hyun-joong Chung,[†,§] Kohji Ohno,[‡] Takeshi Fukuda,[‡] and Russell J. Composto*[,†]

Materials Science and Engineering and Laboratory for Research on the Structure of Matter, University of Pennsylvania, Philadelphia, Pennsylvania 19104-6272, and Institute for Chemical Research, Kyoto University, Uji, Kyoto 611-0011, Japan

Received September 1, 2006; Revised Manuscript Received October 26, 2006

ABSTRACT: We present experimental results showing that roughening in polymer blend films is driven by the underlying phase-separated morphology. To control morphology and stability, nanoparticles (NP) are added to poly(methyl methacrylate) (PMMA):poly(styrene-*ran*-acrylonitrile) (SAN) (50:50) films having a thickness of 550 nm. These PMMA:SAN films undergo symmetric wetting with PMMA layers at the surface and substrate and separate into PMMA-rich (A) and SAN-rich (B) coexisting phases. Three varieties of NP are investigated and either partition into A (NP_A) or segregate weakly (NP_w) or strongly (NP_s) to the interface between A and B. Using scanning force microscopy, the surface roughness is monitored for films containing up to 20 wt % NP. Whereas rupture is observed in neat blends and blends with NP_w or NP_A, stable films are produced by the addition of only 2 wt % NP_s. Although capillary fluctuations fail to predict roughening, a novel model based on the Laplace pressure produced by the internal morphology agrees with experimental results. For neat blends and blends with NP_A, long wavelength fluctuations exhibit universal scaling with roughness, $\lambda_s \propto R_q^{1/4}$. Although the origin of this coupling is unknown, we propose that spinodal decomposition during initial phase separation may trigger the long wavelength fluctuations. By identifying the driving force for roughening in nanocomposite films, we can better understand and control high-performance coatings containing incompatible components and functional inorganic additives.

Introduction

Liquid film stability on solid substrates underlies many technologically important processes ranging from paint gloss to the resolution of inkjet printers. Although most coatings are multicomponent and multiphase, roughening and rupture mechanisms are not understood. For single-layer[1−7] and multilayer[8−11] homogeneous films, capillary fluctuations produced by long-range van der Waals forces[1,4,6−8,11] or external stimuli, e.g., electric field,[3,5,10] can destabilize films, whereas the Laplace pressure, which resists interfacial deformation, can stabilize the films. For polymer blends undergoing phase separation, Hoppe et al.[12] found that the rupture time τ_r and the periodicity of fluctuations at rupture $\lambda_{s,r}$ scaled linearly with film thickness d. In these experiments, the driving force for destabilization was unclear. Recently, Clarke[13,14] suggested that lateral compositional fluctuations, due to phase separation, destabilize polymer blend films.

Before investigating roughening in polymer blend films, the structural evolution proceeding rupture must be understood. For A/B blends where A wets the free surface and substrate, three distinct stages of evolution are observed after a critical quench.[15] The early stage is characterized by rapid growth of wetting layers concurrent with the formation of a three-dimensional (3D) bicontinuous structure in the midlayer.[16] At the onset of the intermediate stage, this 3D structure evolves into discrete, circular domains of A that span the B midlayer.[17] In the late stage, long wavelength (order 10 μm) interfacial fluctuations cause the film to rupture.[18] The origin of these fluctuations is unknown. These previous studies of A/B blends provide the starting point for understanding the mechanism of roughening in liquid films.

In this paper, we provide experimental evidence that the Laplace pressure induced by a phase-separated structure provides the driving force for roughening and rupture in neat polymer blend (A/B) films and those containing nanoparticles (NP). The NP systems are designed to either partition into A (NP_A) or weakly (NP_w) or strongly (NP_S) segregate to the interface between phases. During phase separation, roughened films display periodic, lacey structures, similar to a spinodal dewetting pattern. Whereas NP_w inhibit roughening more than NP_A, NP_s prevent film rupture at concentrations as low as 2 wt %. The periodicity of fluctuations scales with roughness as $\lambda_s \propto R_q^{1/4}$ for neat blends and blends containing NP_A, whereas scaling breaks down for blends containing NP that segregate to the interface, namely NP_w and NP_S.

Experimental Methods

Deuterated poly(methyl methacrylate) (A) and poly(styrene-*ran*-acrylonitrile) (B), from Polymer Sources and Monsanto, respectively, have weight-average molecular weights (M_w) and polydispersities (PDIs) of 106 000 and 1.20 and 118 000 and 2.24, respectively. This blend exhibits a lower critical temperature of ~160 °C. At 195 °C, the coexisting compositions are nearly pure A and B.[15] The three NP have distinct surface functionalities that control their segregation behavior. NP_A are colloidal silica particles (Nissan Chemical) with a diameter of 22 nm and a surface with methyl and hydroxyl groups.[19,20] NP_w and NP_s, denoting weakly and strongly segregating particles, have a silica core (Nissan Chemical) with a slightly smaller diameter (15 nm). These NP's are grafted with PMMA brushes having M_w's of 23 700 and 2100, respectively. As discussed in ref 21, NP_A distribute throughout phase A, NP_w are found in phase A and at the A/B interface, and NP_s locate only at the A/B interface. The A/B blend (50/50) and NP's

† University of Pennsylvania.
‡ Kyoto University.
§ Present address: Samsung SDI, Korea.
* Corresponding author: phone (215) 898-4451; fax (215) 573-2128; e-mail composto@lrsm.upenn.edu.

10.1021/ma062024h CCC: $37.00
Published on Web 12/24/2006

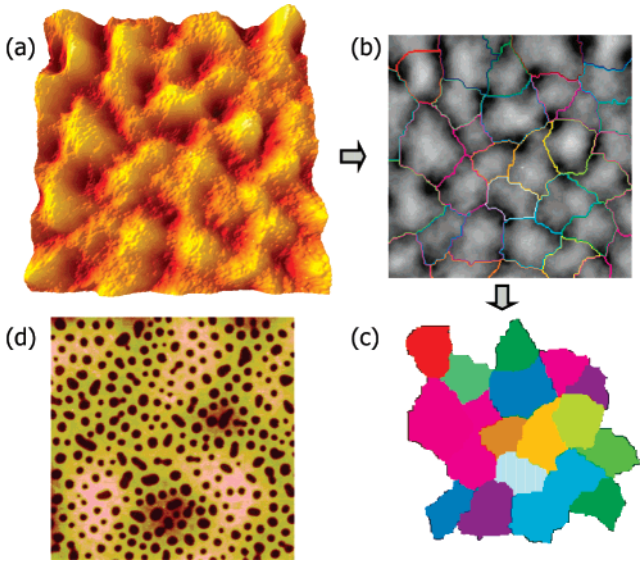

Figure 1. A demonstration of the analysis method used to quantify the surface (a−c) and midlayer (d) features in SFM images. This particular film contains 2 wt % NP_w and is annealed for 24 h. The RMS roughness (R_q) is obtained from the image (100 μm) in (a). (b) Watershed segmentation is used to distinguish the boundaries between peaks. (c) Omitting patches around the edge of (b), the fluctuation wavelength (λ_s) is determined from the mean diameter of each colored patch. (d) The midlayer morphology (40 μm) consists of the continuous B phase (light) and domains of A (dark circles). For this sample, the roughness, wavelength fluctuation and correlation length are R_q = 42 nm, λ_s = 18 μm, and ξ = 2.32 μm.

were mixed in methyl isoamyl ketone, spun-cast on silicon, and dried at 120 °C in a vacuum for 24 h. The film thickness was d = 550 nm. Films were annealed on a hot stage (FP-82, Mettler Toledo) at 195 °C in argon. The surface and midlayer morphologies were characterized using a Dimension 3000 SFM (Veeco Inc.) driven in tapping mode. To reveal the interface morphology of B, A was removed by exposing films to 2.85 MeV He^{2+} ions and then rinsing with acetic acid.[15−18]

Results

Roughening was evaluated by following the evolution of the surface and interface morphology. As an example of the image analysis procedure, Figure 1 shows the surface and the midlayer morphology of a film with 2 wt % NP_w after a 24 h anneal. First, the topography of the surface is projected as a 3D image, as shown in Figure 1a. The surface fluctuation wavelength λ_s is determined by measuring the mean diameter of the area for each high region. Using SPIP software (Image Metrology Inc.), a watershed segmentation algorithm[22] then divides the image into regions as shown in Figure 1b. The same cutoff values are used for surfaces having a similar roughness. As roughness increases, larger cutoff values are required to remove high-frequency noise. Partly imaged regions near the edge are omitted as shown in Figure 1c. From this image, λ_s is determined from the mean diameter of a circle having the same area as the original irregularly shaped region. For the internal or midlayer morphology shown in Figure 1d, the correlation length ξ between A domains (dark) was determined from the dominant wavevector, $k_{max}(t)$, by converting the image into reciprocal space by a fast-Fourier transform and using $\xi(t) = 2\pi/k_{max}(t)$.

Surface roughening and rupture can be slowed down or even prevented by the addition of NP as dramatically illustrated in Figure 2. Figure 2a shows that neat blend films are extremely rough and exhibit a root-mean-square (rms) roughness (R_q) of 506 nm after 72 h. Upon adding 5 wt % NP_A or NP_w, films are smoother as shown by parts b and c of Figure 2, respectively.

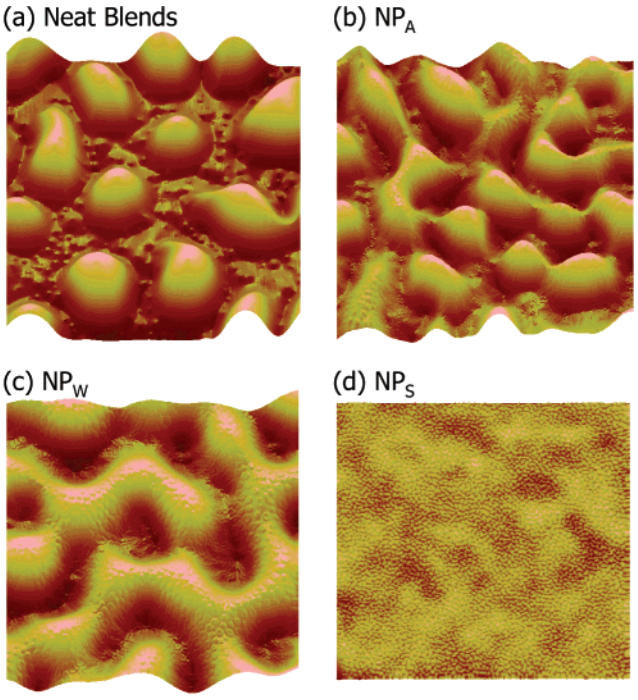

Figure 2. Surface SFM images (100 μm) of films without (a) and with 5 wt % NP (b−d). Annealing times and z ranges are 72 h and ±1500 nm (a) or 120 h and ±750 nm (b−d). For (a−d), the rms roughness values are 506, 223, 167, and 7 nm, respectively. For (a−d), the fluctuations have wavelengths of 30, 22, 26, and 14 μm, respectively.

With respect to the neat blend, the R_q values are lower, 223 and 167 nm, respectively, even though films are annealed for a longer time, 120 h. However, the addition of 5 wt % NP_A or NP_w does not prevent rupture. In contrast, films with 5 wt % NP_s are remarkably stable and very smooth (R_q = 7 nm) as shown by Figure 2d. As shown below, the driving force for film roughening can be understood by analyzing R_q and λ_s.

Figure 3 shows how R_q evolves with time for the neat blend (closed triangles) and blends containing 2−20 wt % NP. By observing that hazy (rough) films display R_q values >100 nm, a rupture time τ_r is empirically defined by $R_q(\tau_r)$ = 100 nm. Applying this definition to Figure 3a, τ_r is ∼14 h for neat blends and ∼24, ∼36, and ∼76 h for 2, 5, and 10 wt % NP_A, respectively. The increase in τ_r with NP_A loading is attributed to an increase in the viscosity of the A phase, as previously described.[23] Whereas films containing 2 and 5 wt % NP_w rupture after ∼50 and ∼60 h, respectively, the addition of 10 and 20 wt % NP_w produces stable films for at least 120 h, as shown in Figure 3b. Remarkably, film stability is achieved by the addition of only 2 wt % NP_s as shown in Figure 3c. This result is consistent with our recent observation that the internal phase structure can be pinned by jamming of NP_s at the interface.[21]

Figure 4 shows how λ_s evolves with time for the neat blend and blends containing 2−20 wt % NP. Initially, all films are smooth ($R_q \approx$ 5 nm), and no periodic fluctuations are observed. For the shortest annealing time, 1 h, all samples have similar λ_s values, ca. 8 μm. For blends with NP_A, λ_s monotonically increases as time increases and, after 120 h, approaches 21, 22, and 20 μm for 2, 5, and 10 wt % loadings, respectively. As shown in Figure 3a, R_q increases in a similar manner before reaching ∼321, ∼228, and ∼206 nm at 120 h, respectively. On the other hand, for blends with NP_s, λ_s values are shorter and reach only ∼13, ∼12, and ∼9 μm, respectively, consistent with the much smaller R_q values of ∼11, ∼8, and ∼5 nm shown in Figure 3c. However, for blends containing 20 wt % NP_w,

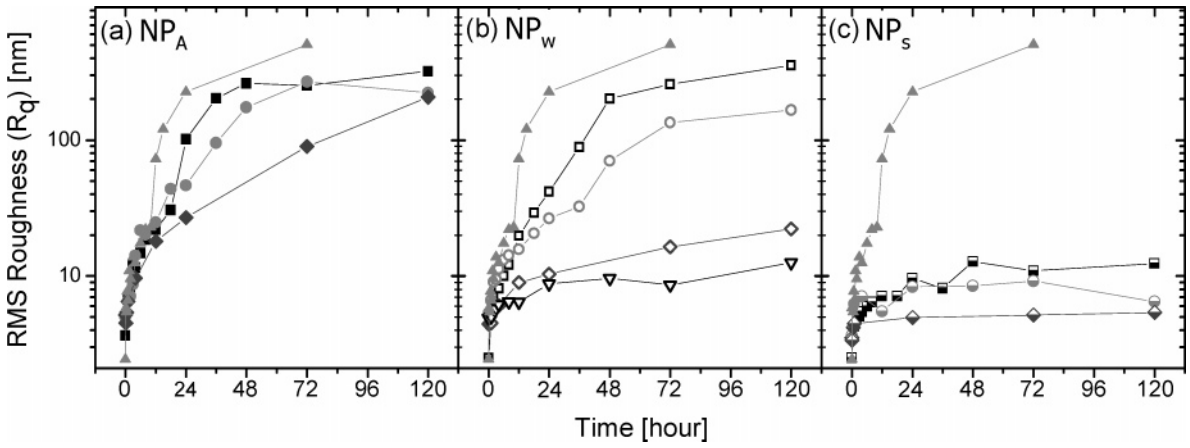

Figure 3. Evolution of rms roughness (R_q) plotted vs time. Rupture time is defined when $R_q = 100$ nm. The solid upper triangles (without NP) are included in all three figures as a reference. Squares, circles, diamonds, and lower triangles correspond to 2, 5, 10, and 20 wt % NP loadings, respectively. The same symbol identifications are used in Figures 4 and 5.

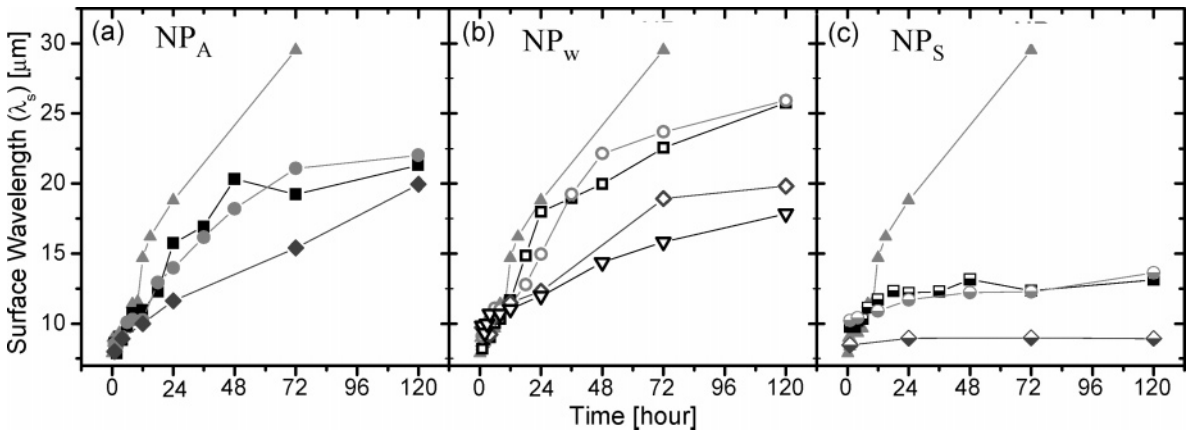

Figure 4. Surface fluctuation wavelength (λ_s) vs time for the three types of NP. Symbols are described in the caption of Figure 3. See text for details.

between 24 and 120 h, λ_s increases from 12 to 18 μm. However, R_q is nearly invariant, only increasing slightly from 9 to 13 nm, suggesting that the wavelength and local roughness are decoupled. This observation is discussed later.

Discussion

Capillary fluctuations along the interface between the wetting and midlayer is a potential driving force for film roughening. In the layered structure A/A:B/A/substrate, deformation along the A/A:B interface can dominate roughening because the interfacial tension ($\sigma_i = 0.9$ mJ/m^2) is much less than the surface tension ($\sigma_s = 27.4$ mJ/m^2).[15] If a long-range van der Waals force produces interfacial fluctuations, λ_s and τ_r are given by $\lambda_s = 4\pi d^2(\pi\sigma_s/A_H)^{1/2}$ and $\tau_s = (48\eta\pi^2\sigma_s/A_H^2)d^5$, where A_H and η are the Hamaker constant and viscosity, respectively.[1] Using literature and measured values for $A_H \approx 10^{-19}$ J and $\eta_B \approx 4.0 \times 10^3$ Pa•s,[6,24] respectively, and the d value for the entire film, 550 nm, τ_s and λ_s are 169 years and 530 μm, respectively. Clearly these predictions are inconsistent with the experimental results in Figure 3, which indicate $\tau_s \approx 1$ day and $\lambda_s \approx 10$ μm. Here, we present a new model that is consistent with the phase-separated morphology prior to rupture and attributes film rupture to the Laplace pressure produced by the internal structure in the midlayer.

In our system, the Laplace pressure can stabilize or destabilize the film. The stabilizing Laplace pressure results from the surface curvature (ΔP_s), which comes from long-range fluctuations along x and z directions (cf. Figure 5), namely, λ_s and R_q, respectively. Approximating the surface fluctuation as a sinusoidal function, the stabilizing pressure is

$$\Delta P_s = \frac{2(\sigma_s + \sigma_i)}{r_s} = \frac{16}{\sqrt{\pi}}\frac{(\sigma_s + \sigma_i)R_q}{\lambda_s^2} \quad (1)$$

where the radius of curvature, $r_s = (\sqrt{\pi}/8)(\lambda_s^2/R_q)$. The destabilizing pressure from the internal structure (ΔP_i) is indicated in sketches of the morphology shown in Figure 5a,b. By designating the surface height and period as $h(x) = d \pm R_q$ and λ_s, respectively, the number of A domains per thin region is $(\lambda_s/\xi)^2/2$. Neglecting thin wetting layers, the radius of curvature for the B phase (gray in Figure 5) in the thin region is $r_1 = (d - R_q)/2$. Similarly, in the thick region, $r_2 = (d + R_q)/2$. Therefore, the internal pressure difference between the thin and thick regions can be approximated as

$$\Delta P_i = \sigma_i\left[\frac{1}{r_1} - \frac{1}{r_2}\right]\left(\frac{\lambda_s}{\xi}\right)^2 \cong \sigma_i\left[\frac{4R_q}{d^2 - R_q^2}\right]\left(\frac{\lambda_s}{\xi}\right)^2 \quad (2)$$

For $\Delta P_i > \Delta P_s$, B flows from depressed to elevated regions as illustrated by the arrow below Figure 5b. This flow amplifies the long-wavelength fluctuations and increases film roughness. In this treatment, the flow of B will decrease the amount of B in the thin region (B phase shrinks) and increase B in the thick region (expands). Conversely, A domains will expand and shrink within the thin and thick regions, respectively.

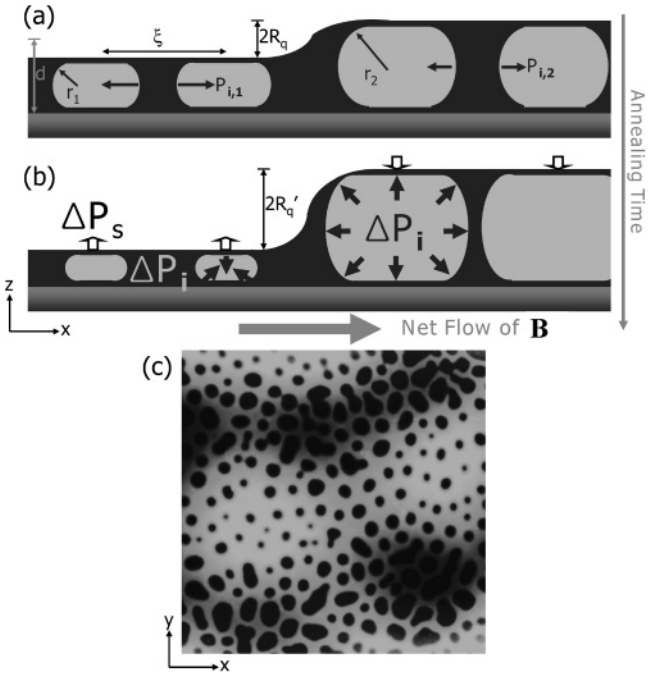

Figure 5. (a, b) Two sequential cartoons of the internal structure and film thickness that depict the late stage morphology evolution where fluctuations in film thickness facilitate rupture. The internal structure exerts a Laplace pressure that destabilizes the film by amplifying long-wavelength fluctuations. Black and gray corresponds to A and B phases, respectively. Because of the higher curvature of the B phase in thin regions ($r_1 < r_2$), the Laplace pressure is greater in the thin regions ($P_{i,1} > P_{i,2}$). Thus, B flows from depressed to elevated regions because of the internal Laplace pressure gradient (ΔP_i), resulting in amplification of long-wavelength fluctuations. Evidence for this mechanism is presented by the SFM image (40 μm × 40 μm) of the midlayer for a blend with 5 wt % NP_w after 72 h (c). Here, the light and dark regions correspond to high and low points, respectively, whereas the black circles are A domains (etched). Note that the B phase is continuous, although B appears discrete in (a) and (b). The same gray and black color schemes are used in (a), (b), and (c). R_q, λ_s, and ξ are 134.6 nm, 23.7 μm, and 2880 nm, respectively.

Using measured characteristics, the proposed model can be tested by determining whether $\Delta P_i > \Delta P_s$. For neat blends at 10 h, λ_s, R_q, and ξ are 11 μm, 22 nm, and 2600 nm, respectively. Using eqs 1 and 2, ΔP_s and ΔP_i are 47 N/m^2 and 5700 N/m^2, respectively. Because ΔP_i is about 125 times larger than ΔP_s, the internal Laplace pressure can drive B from depressed to elevated regions (i.e., arrow pointing toward $+x$), causing roughness amplification. For a neat bend and blends containing NP_A at 2, 5, and 10 wt %, ΔP_i is consistently about 2 orders of magnitude greater than ΔP_s. Thus, experimental support for the proposed mechanism is rather extensive. In addition, the SFM image in Figure 5c provides direct evidence that B flows from low (dark) to high (light) regions. Note that A domains (dark circles) exhibit larger diameters in thin regions and smaller ones in thick regions, consistent with the sketch in Figure 5b.

For the first time, a destabilization model consistent with the underlying morphology is proposed for roughening in phase-separating polymer blend films. Nevertheless, improvements to this model are possible. For example, the curvature of the B phase in the $x-z$ plane produces flow over a distance λ_s. An improved model would also capture local flow of B over the distance ξ, which is generated by curvature along the $x-y$ plane defined in Figure 5c. As described in an earlier study, this curvature drives domain coalescence.[17,25]

Having quantified roughening using λ_s and R_q, an investigation of coupling between these key parameters may further elucidate the origin of roughening. Figure 6 shows λ_s vs R_q for A/B films and those containing NP. For neat and NP_A blend films, a scaling relation (solid line) is observed, λ_s [nm] = $5000R_q^{0.25}$, for R_q ranging from ~6 to ~300 nm, as shown in Figure 6. However, scaling breaks down for films containing NP that segregate to the interface, as shown in the inset of Figure 6. This result indicates that film roughening is perturbed (i.e., λ_s and R_q are decoupled) by NP segregation to the interface. Specifically, λ_s increases more rapidly than R_q as shown by the data in the inset. Qualitatively, the origin of this scaling breakdown is likely related to the prolonged film stability observed when NP locate at the interface. However, new experiments and theory are needed for a complete description.

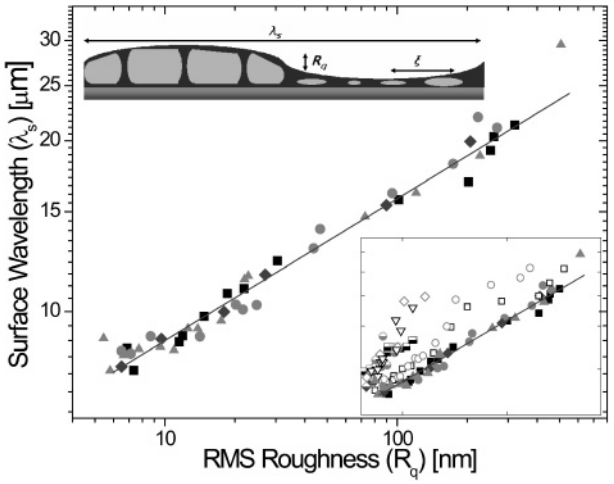

Figure 6. A log−log plot of λ_s vs R_q. The symbols follow Figure 3. For neat blend films and films containing NP_A, λ_s scales with $R_q^{1/4}$. (lower inset) For films with NP_w or NP_S, scaling breaks down, suggesting that NP at the interface perturb the growth of interfacial fluctuations that lead to film rupture. (upper inset) Cross-sectional cartoon depicting the internal structure of the film and key parameters λ_s, R_q, and ξ. Black and gray correspond to A and B phases, respectively.

To understand the scaling relation uncovered in Figure 6, the origin of long-range fluctuations must be known. Although a definitive answer is lacking, the recent theory by Clarke,[13] which attributes film destabilization to inhomogeneities in lateral composition, may shed some light on the observed scaling behavior. In our system, we postulate that short-wavelength composition fluctuations produced by spinodal decomposition (i.e., early stage) induce the long-wavelength surface fluctuation in Figure 5. Interestingly, the initiation of a long-wavelength fluctuation by a short-wavelength fluctuation has been observed in the wrinkling of a metal layer on a polymer film[26] as well as Turing and spiral waves in chemical reactions.[27] We hope that our new experimental results will stimulate new theories of roughening in liquid thin films.

Conclusion

In this paper, film roughening is investigated in neat blends as well as those containing NP. If they segregate to the interface, NP can jam together and prevent film rupture. Although particle stabilization in emulsions is of longstanding interest, recent interest in new nanoscale materials has driven a resurgence in understanding the behavior of NP at interfaces.[28] New models[29] have appeared as well as the observation of interconnected glasslike structures.[30] The main result of this paper is that internal phase separation destabilizes multicomponent, complex, liquid films by a morphology-driven Laplace pressure. The long-wavelength fluctuation that drives dewetting of the polymer

blend films may be initiated by short-wavelength fluctuations resulting from spinodal decomposition. The scaling relation $\lambda_s \propto R_q^{1/4}$ is an interesting finding that will hopefully motivate new theories of dewetting that describe polymer blend and nanocomposite liquid films. The proposed model can be extended to polymer blend films showing asymmetric wetting[31] in addition to the symmetric wetting case explored in the current paper.

Acknowledgment. This work was supported by NSF DMR-(05-49307), NSEC(04-25780), and MRSEC(05-20020) programs. We thank Professor Tom Lubensky for insightful discussions.

References and Notes

(1) Brochard Wyart, F.; Daillant, J. *Can. J. Phys.* **1990**, *68*, 1084−1091.
(2) Carson Meredith, J.; Smith, A. P.; Karim, A.; Amis, E. J. *Macromolecules* **2000**, *33*, 9747.
(3) Pease, L. F. III; Russel, W. B. *J. Non-Newtonian Fluid Mech.* **2002**, *102*, 233.
(4) Reiter, G.; Khanna, R.; Sharma, A. *J. Phys.: Condens. Matter*. **2003**, *15*, S331−S336.
(5) Schaffer, E.; Thurn-Albrecht, T.; Russell, T. P.; Steiner, U. *Europhys. Lett.* **2001**, *53*, 518.
(6) Seemann, R.; Herminghaus, S.; Jacobs, K. *Phys. Rev. Lett.* **2001**, *86*, 5534.
(7) Vrij, A.; Oberbeek, J. Th. G. *J. Am. Chem. Soc.* **1968**, *90*, 3074.
(8) Brochard Wyart, F.; Martin, P.; Redon, C. *Langmuir* **1993**, *9*, 3682.
(9) Faldi, A.; Composto, R. J.; Winey, K. I. *Langmuir* **1995**, *11*, 4855.
(10) Lin, Z.; et al. *J. Chem. Phys.* **2001**, *114*, 2377.
(11) Sferrazza, M.; et al. *Phys. Rev. Lett.* **1998**, *81*, 5173.
(12) Hoppe, H.; Heuberger, M.; Klein, J. *Phys. Rev. Lett.* **2001**, *86*, 4863.
(13) Clarke, N. *Eur. Phys. J. E* **2004**, *14*, 207.
(14) Clarke, N. *Macromolecules* **2005**, *38*, 6775.
(15) Wang, H.; Composto, R. J. *J. Chem. Phys.* **2000**, *113*, 10386.
(16) Wang, H.; Composto, R. J. *Phys. Rev. E* **2000**, *61*, 1659.
(17) Chung, H.-J.; Composto, R. J. *Phys. Rev. Lett.* **2004**, *92*, 185704.
(18) Wang, H.; Composto, R. J. *Macromolecules* **2002**, *35*, 2799.
(19) Yoshitake, K.; Yokoyama, T. Process of Producing Hydrophobic Organosilica Sol. Nissan Chemical Inc. US Patent 60025455A, 2000.
(20) Liu, Y.-L.; Li, S.-H. *Macromol. Rapid Commun.* **2004**, *25*, 1392.
(21) Chung, H.-J.; Ohno, K.; Fukuda, T.; Composto, R. J. *Nano Lett.* **2005**, *5*, 1878.
(22) Russ, J. C. *The Image Processing Handbook*, 4th ed.; CRC Press: Boca Raton, FL, 2002.
(23) Chung, H.-J.; Taubert, A.; Deshmukh, R. D.; Composto, R. J. *Europhys. Lett.* **2004**, *68*, 219.
(24) Zhang Newby, B.-M.; Composto, R. J. *Macromolecules* **2000**, *33*, 3274.
(25) Tanaka, H. *J. Phys.: Condens. Matter* **2001**, *13*, 4637.
(26) Yoo, P. J.; Lee, H. H. *Phys. Rev. Lett.* **2003**, *91*, 154502.
(27) Yang, L.; Dolnik, M.; Zhabotinsky, A. M.; Epstein, I. R. *J. Chem. Phys.* **2002**, *117*, 7259.
(28) Binks, B. P. *Curr. Opin. Colloid Interface Sci.* **2002**, *7*, 21.
(29) Stratford, K.; Adhikari, R.; Pagonabarraga, I.; Desplat, J.-C.; Cates, M. E. *Science* **2005**, *309*, 2198.
(30) Manley, S.; et al. *Phys. Rev. Lett.* **2005**, *95*, 238302.
(31) Keblinski, P.; Kumar, S. K.; Maritan, A.; Koplik, J.; Banavar, J. R. *Phys. Rev. Lett.* **1996**, *76*, 1106.

MA062024H